3D Printing/Interfacial Polymerization Coupling for the Fabrication of Conductive Hydrogel

Postfach 10 11 61
69451 Weinheim
Germany
Courier services:
Boschstraße 12
69469 Weinheim
Germany
Tel.: (+49) 6201 606 581
Fax: (+49) 6201 606 510
E-mail: macromol@wiley-vch.de

WILEY-VCH

Dear Author,

Please correct your galley proofs carefully and return them no more than four days after the page proofs have been received.

The editors reserve the right to publish your article without your corrections if the proofs do not arrive in time.

Note that the author is liable for damages arising from incorrect statements, including misprints.

Please note any queries that require your attention. These are indicated with a Q in the PDF and a question at the end of the document.

Please limit corrections to errors already in the text; cost incurred for any further changes or additions will be charged to the author, unless such changes have been agreed upon by the editor.

Reprints may be ordered by filling out the accompanying form.

Return the reprint order form by fax or by e-mail with the corrected proofs, to Wiley-VCH : macromol@wiley-vch.de

To avoid commonly occurring errors, please ensure that the following important items are correct in your proofs (please note that once your article is published online, no further corrections can be made):

- **Names** of all authors present and spelled correctly
- **Titles** of authors correct (Prof. or Dr. only: please note, Prof. Dr. is not used in the journals)
- **Addresses** and **postcodes** correct
- **E-mail address** of corresponding author correct (current email address)
- **Funding bodies** included and grant numbers accurate
- **Title** of article OK
- All **figures** included
- **Equations** correct (symbols and sub/superscripts)

Corrections should be made directly in the PDF file using the PDF annotation tools. If you have questions about this, please contact the editorial office. The corrected PDF and any accompanying files should be uploaded to the journal's Editorial Manager site.

Q1 xxxx

E. Fantino,* I. Roppolo, D. Zhang, J. Xiao, A. Chiappone, M. Castellino, Q. Guo, C. F. Pirri, J. Yang* 1700356

3D Printing/Interfacial Polymerization Coupling for the Fabrication of Conductive Hydrogel

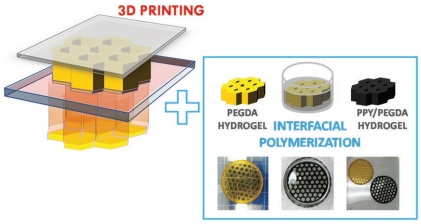

3D printing is coupled with interfacial polymerization to obtain electroactive hydrogels with complex and defined geometry. Conductive hydrogels are created through a two-step procedure: first a digital light processing 3D printing system is used to fabricate 3D structures and then pyrrole is oxidized to polypyrrole, exploiting an interfacial polymerization mechanism, thus creating a conductive phase directly in 3D printed structure.

Macromolecular Materials and Engineering
www.mme-journal.de

3D Printing/Interfacial Polymerization Coupling for the Fabrication of Conductive Hydrogel

Erika Fantino, Ignazio Roppolo, Dongxing Zhang, Junfeng Xiao, Annalisa Chiappone, Micaela Castellino, Qiuquan Guo, Candido Fabrizio Pirri, and Jun Yang**

In this study, 3D printing is coupled with interfacial polymerization to obtain electroactive hydrogels with complex and defined geometry. Conductive hydrogels are created through a two-step procedure: first a digital light processing 3D printing system is used to fabricate poly(ethylene glycol)diacrylate 3D structure and then pyrrole is oxidized to polypyrrole (PPY), exploiting an interfacial polymerization mechanism thanks to which PPY can be formed into the poly(ethylene glycol) matrix, thus creating a conductive phase.

1. Introduction

Recently, conductive hydrogels have attracted much interest in the field of biomaterials science being able to combine highly hydrated polymer structures with intriguing electronic functionalities.[1,2] These hybrid materials, merging the hydrogel characteristics with the advantages of the conductive components such as electrical conductivity and electrochemical-redox properties, have found applications across a range of biomedical applications such as biosensors, drug delivery, and tissue engineering.[3,4] In these composite hydrogels, conductivity was achieved either incorporating electrically conductive fillers, such as graphite, metallic particles, and carbon nanotubes,[5–7] or integrating intrinsically conductive polymers within the hydrogel matrix.

Conductive polymers are macromolecules with conjugated backbone; examples are polyacetylene, polythiophene, polypyrrole (PPY), or polyaniline. In recent years they have received great interest owing to their ability to conduct electricity and they have been used in several biomedical applications.[4,8–11]

E. Fantino, Prof. C. F. Pirri
Department of Applied Science and Technology
Politecnico di Torino
Corso Duca degli Abruzzi 24, Torino 10129, Italy
E-mail: erika.fantino@polito.it
I. Roppolo, A. Chiappone, M. Castellino, Prof. C. F. Pirri
Center for Sustainable Futures@Polito
Istituto Italiano di Tecnologia
Corso Trento 21, Torino 10129, Italy
D. Zhang, J. Xiao, Q. Guo, Prof. J. Yang
Department of Mechanical and Materials Engineering
The University of Western Ontario
London, Ontario, N6A 5B9, Canada
E-mail: jyang@eng.uwo.ca
The ORCID identification number(s) for the author(s) of this article can be found under https://doi.org/10.1002/mame.201700356.

DOI: 10.1002/mame.201700356

Conductive hydrogels exploiting intrinsically conducting polymers allow obtaining materials that further expand the application area of hydrogels[12–14] driving researchers to develop new fabrication methods.

The fabrication of conductive hydrogels with particular geometry and controlled features is still a big issue. 3D printing is an additive manufacturing (AM) process that enables to construct 3D objects directly from a digital model. It has received a great deal of attention from a diverse range of fields including electronics,[14] biomedics and regenerative medicine,[15–17] and microfluidics.[18] Objects are constructed layer-by-layer, enabling the creation of complex parts with tailored morphology and functionality.[19] There exist several different 3D printing techniques that differ from each other for the kind of polymer that is used (i.e., thermoplastic or thermosetting) and for the technology beyond the building process.[16] One of the most widely used 3D printing processes, namely, vat polymerization, is based on photopolymerization. Stereolithography (SLA), a well-established AM technology, is used to create thermoset objects with features <100 μm by selectively scanning an ultraviolet (UV) laser beam across a reservoir of photopolymer resin.[19] Another 3D printing process based on spatially controlled solidification of a liquid resin by photopolymerization is digital light processing (DLP). Instead of using a laser to "draw" the object under a point-by-point manner like in SLA, DLP equipment projects an entire slice of an object using a digital projector.[20] Both techniques provide powerful tools to fabricate complex 3D polymeric structures, with good resolution and fast production times especially in the case of DLP. This opens infinite possibilities in their design and applications.[21–25]

Many types of hydrogels have been reported in the literature including natural materials or synthetic ones.[16,26,27] Among the synthetic polymers, poly(ethylene glycol) (PEG) based ones have been used extensively for the fabrication of hydrogels thanks to their well-known hydrophilicity and biocompatibility.[28,29] With acrylated or methacrylated moieties, PEG monomers can be photocrosslinked in the presence of appropriate initiating agents and the use of SLA or DLP has also been reported as a successful method for fabricating complex functional 3D structures based on PEG monomer materials.[23,30–33] The choice of relatively low molecular weight (M_w 500–700) PEG-based acrylate monomers allows preparing ractive formulations with sufficietly low viscosity to be processed with a fast and low-cost DLP apparatus giving self-standing and robust

structures thanks to the crosslinkind density reached in this kind of network.[34] Herein, the strategy we developed within this study consists in coupling interfacial polymerization[8,35–37] with 3D printing in order to obtain electroactive hydrogel with complex and defined geometry. After 3D printing of the hydrogel structures, a chemical oxidative polymerization of pyrrole (PY) was performed for preparing conductive hydrogels. By tuning the reaction conditions, the conductive components can permeate spontaneously and exclusively into the hydrogels to achieve required conductivity.[5,38–40]

Moreover the dye used for obtaining the 3D printed structures was employed as dopant for PPY, enhancing the electrical conducitvity.[6,41,42] If compared with other methods proposed in the literature,[12,13,43] this two-step approach can provide a higher control over the structure of the conductive hydrogel thanks to the formation of the conductive phase in a dedicated step that allows maintaining the defined 3D microarchitecture of the printed hydrogel, bringing to very precise and complex structures with electrical features. This approach has the potential to be extended to a wide variety of photosensitive hydrogels. The proposed strategy, coupling hydrogels, 3D printing, and conductive polymers, could open new paths for the development of new bioelectrical interfaces for several biomedical applications, like complex systems for drug delivery or scaffolds for regenerative medicine but also in bioenergy fields or sensors.

2. Experimental Section

2.1. Materials

Poly(ethylene glycol)diacrylate (PEGDA) with a molecular weight of 700 g mol^{-1} and PY reagent grade 98% were purchased from Sigma-Aldrich and used as received. Phenylbis(2,4,6-trimethylbenzoyl)phosphine oxide, selected as photoinitiator (PI) for its fair absorbing characteristics in the deep blue to near UV, and the dye, methyl orange (MO), were purchased from Sigma-Aldrich and used as received. Iron(III) chloride hexahydrate ($FeCl_3$ $6H_2O$) was purchased from Alfa Aesar.

2.2. Fabrication of 3D PPy/PEGDA Structure

3D printable mixtures containing PEGDA, MO 0.2 phr (per hundred resin), and distilled water (dH_2O) in different concentration (40, 50, 60, and 70% w/w) were prepared. 2 phr PI with respect to the PEGDA amount was added in the formulation. The 3D printing was performed on a PICOplus39, Asiga, with an X-Y resolution of 39 µm and light intensity of 30 mW cm^{-2}. The digital models of structures were designed and converted to sterolithography (STL) file format for 3D printing. The layer thickness was set to 25 µm and the exposure time varied from 2 to 15 s for increasing amounts of water.

Pyrrole monomers were dissolved in cyclohexane (0.5 M PY) while ferric chloride was dissolved in deionized water (0.3 M $FeCl_3$). First the 3D parts were soaked for 1 h in the aqueous solution containing ferric chloride. The hydrogel was then carefully blotted and subsequently soaked in the organic solution containing the pyrrole monomers. The monomer pyrrole and the oxidant $FeCl_3$ diffuse at the aqueous/organic interface, the polymerization occurs, and the PPY/PEGDA composite hydrogel is formed. The same procedure was conducted on the thin film for electrical measurement.

2.3. Characterization Methods

Real-time rheological measurements were performed using an Anton Paar rheometer (Physica MCR 302) in parallel plate mode with a Hamamatsu LC8 lamp with a visible bulb and a cutoff filter below 400 nm (light intensity was set to 30 mW cm^{-2}). The UV curing set up is equipped with a lower plate in quartz that allows the irradiation of the sample during the measurement. The gap between the two plates was set to 0.1 mm and the sample was kept at a constant temperature (25 °C) and under constant shear frequency of 10Hz, light was turned on after 120 s in order to stabilize the system. Concomitant changes in viscoelastic material moduli during polymerization were measured as a function of exposure time. The experiment was performed in the linear viscoelastic region with a strain amplitude of 0.5%. The morphological characterization of the 3D printed materials after the interfacial polymerization of PY was carried out by scanning electron microscopy (SEM, Hitachi TM3030Plus). ATR spectra were collected on a Tensor 27 FTIR spectrometer (Bruker). The averaged signal was collected with a resolution of 2 cm^{-1} from 4000 to 400 cm^{-1}. X-ray photoelectron spectroscopy (XPS) was carried out by using a PHI 5000 VersaProbe (Physical Electronics) system. The X-ray source was a monochromatic Al Kα radiation. Depth profile, by means of an Ar+ flux at 2 kV accelerating voltage, was performed on the sample in an alternate mode with sputtering cycles of 1 min each. Spectra were analyzed using Multipak 9.7 software. All core-level peak energies were referenced to C1s peak at 284.5 eV (C—C/C—H) and the background contribution in HR scans was subtracted by means of a Shirley function. Differential scanning calorimetry (DSC) measurements were performed with a Netzsch DSC 204 F1 Phoenix instrument, equipped with a low-temperature probe, between –80 and 60 °C with a heating rate of 10 °C min^{-1} in nitrogen atmosphere. For each sample, the same heating module was applied two times and the final heat flow value recorded during the second heating cycle. The T_g was defined as the midpoint of the heat capacity change observed in the DSC thermogram. Thermogravimetric analysis (TGA) was performed using a Netzsch TG 209 F1 Libra instrument in the range between 25 and 700 °C, with a heating rate of 10 °C min^{-1} in nitrogen. Prior to the measurement all the samples were dried overnight in a vacuum oven in order to avoid the drop of weight relative to the water/moisture eventually present in the sample. Compression tests were carried out using a dynamometer (Deben Microtest) equipped with a load cell of 200N. Alveolar structures were tested, and at least three specimens for each sample were tested. Samples resistivity was measured by using a Keithley-238 High Current Source Measure Unit (voltage range ±10 V, step 0.1 V), realizing a two-point contact setup placing copper electrodes on the two opposite basal sides. The data showed were obtained by multiple

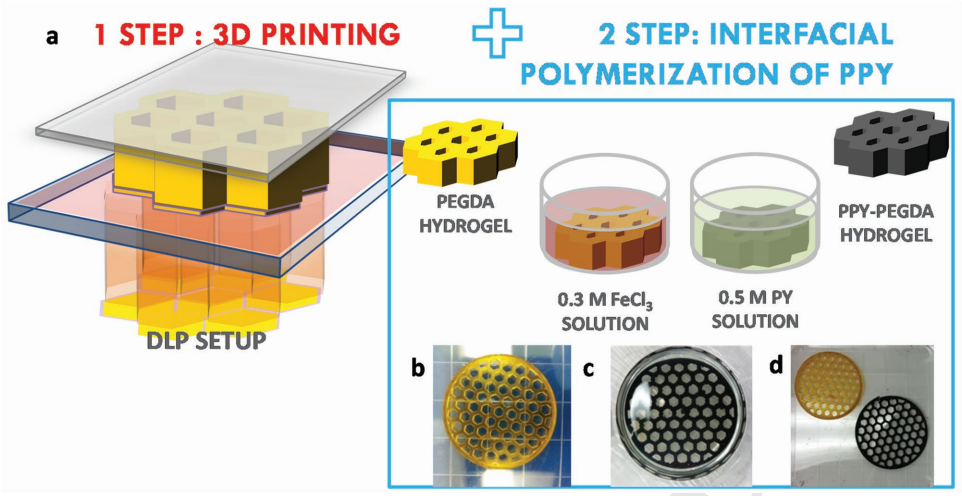

Figure 1. a) Sketch of the process. b) 3D printed PEGDA structure. c) PEGDA structure in PY/CYH solution. d) 3D PEGDA and 3D PEGDA/PPY structures.

measurements on different samples (three for each formulation). The electrical measurements on 3D printed structures were carried out with an apparatus composed of a Keithley 2750 multimeter and realizing a two-point contact setup, placing one copper electrode on each side of the structure.

3. Results and Discussion

In this work hybrid PPY/PEGDA conductive hydrogels were created through a two-step procedure. First a DLP 3D printing system was used to fabricate PEGDA microstructures and then PY was oxidized to PPY, exploiting an interfacial polymerization mechanism. Following this route, PPY could be formed into the PEGDA matrix, thus creating a conductive 3D printed hydrogel (**Figure 1**a).

The developed process is sketched in Figure 1a. 3D PEGDA hydrogel was printed by a DLP machine and then the 3D printed parts were soaked for 1 h in an aqueous solution containing ferric chloride: thanks to the high swell ability of PEGDA networks, the oxidant agent was incorporated in the 3D printed structure. The hydrogels were then carefully blotted and subsequently soaked again in an organic solution containing pyrrole monomers. The polymerization to PPY involves the oxidation of the pyrrole monomer with ferric ions, the pyrrole monomers and the initiator diffuse at the aqueous/organic interface, and thus the polymerization is trigged. The reaction of PY with aqueous ferric chloride ($FeCl_3$) is rapid and the PPY product is in the form of a black powder. After 1 h, the 3D parts are removed from the solution and immersed in dH_2O for at least 1 d to leach out low molecular weight components.

Different hydrogel formulations were prepared; MO was used both as dopant for the PPY[44,45] and as dye to improve the 3D printing resolution.[22–24] dH_2O was added in different amounts (40, 60, and 70% w/w) in the formulations in order to adjust the concentration (**Figure 2**a); the higher is the amount of initial water present in the formulation and, thus in the printed part, the higher will be the hydrogel ability of swelling in the subsequent steps (oxidant solution) and therefore the interfacial polymerization will be probably more efficient. Before printing the formulations, their reactivity was investigated by means of photorheology aiming to check the influence of the high amount of water added to the monomers on the light-induced crosslinking reaction. As expected, the higher the amount of water, the slowest the curing process as shown by the time-dependent elastic modulus (G') values reported in

a

Sample	PEGDA %(w/w)	H_2O %(w/w)	MO (phr)	PI (phr)
PEGDA	100	0	0.2	2
PEGDA_60	60	40	0.2	2
PEGDA_40	40	60	0.2	2
PEGDA_30	30	70	0.2	2

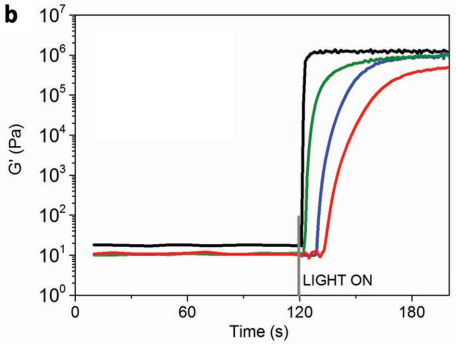

Figure 2. a) 3D printed formulations composition. b) Photorheology characterization of the different formulations.

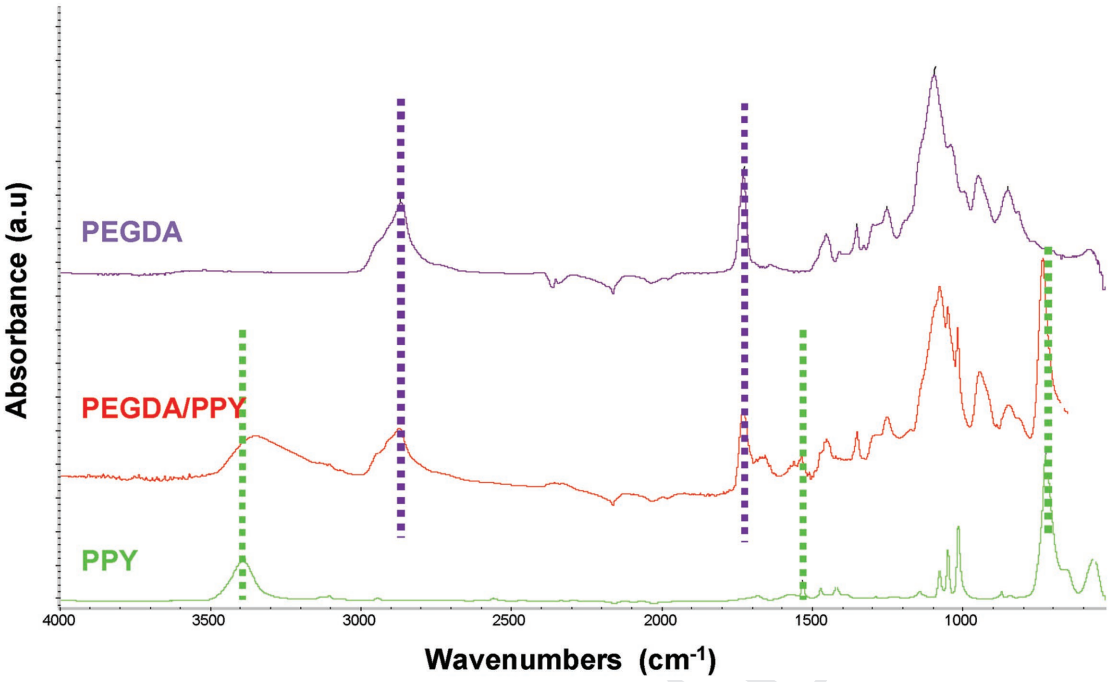

Figure 3. ATR spectra of pure PY (green), PPY/PEGDA hydrogel (red), and PEGDA hydrogel (purple).

Figure 2b. While the *G*' curve relative to neat PEGDA starts increasing almost instantaneously after turning on the light and reaches its postcuring plateau in few seconds, the other formulations show a delay in the beginning of the reaction and a slower kinetic revealed by the lower slope of the curves. This effect results in the need of a longer exposition time during the printing process when the formulations containing higher amounts of water are printed. The use of higher amounts of water also induces a slight reduction of the *G*' modulus after curing; in all the cases the obtained values are in line with those reported for other crosslinked hydrogels measured in similar conditions (amplitude and frequency).[46]

ATR spectroscopy was used to characterize the interfacial polymerization; the spectra are shown in **Figure 3**. The spectrum of neat PPY illustrates absorption peaks at 3402, 1528, 1418, and 1046 cm^{-1} that could be assigned to the N—H, C—C, C—N stretching vibrations, and C—H in-plane vibrational bands of the pyrrole ring, respectively, and the peak at 1309 cm^{-1} is assigned to C—N bonds.[7] In the PEGDA spectrum, the strong peak at 1724 cm^{-1} could be assigned to the —C=O stretching from ester bonds, while the broad band centered at 2862 cm^{-1} can be assigned to the C—H (—CH, $-CH_2$, and CH_3) stretching vibration. In the FTIR of the PEGDA/PPY hydrogel, it is possible to identify characteristic peaks of both polypyrrole, at 3396, 1528, 1465 cm^{-1}, and PEGDA, peak at 1724 and 2862 cm^{-1}, indicating the presence of both polymers blended. This confirms the successful formation of PPY on PEGDA matrix (Figure 3).

Detailed images of 3D printed structures with optical microscopy and SEM are shown in **Figure 4**. Well-defined architecture and good building accuracy of complex objects were achieved; details down to 200 µm were achieved. This value represents the experimental limit observed for this kind of water-based formulations. Moreover, the PPY postpolymerization process on the printed structures does not worsen the resolution achieved during the printing step: the structures in fact remain intact without cracks. The surface after the polymerization of PPY was evaluated by SEM. While the surface of PEGDA structures is smooth, a certain roughness was evident after PPY polymerization, with a flowerlike pattern and big porosity (Figure 4c). Probably this could be related to the high concentration of PY monomers in the solution, which leads to a faster polymerization rate and thus a more uneven distribution of PPY.[47] Thicker samples (4 mm) were also produced and their cross section was observed by SEM analyses in order to evaluate the PPY distribution into the sample. As visible in Figure 4d,e, PPY forms spherical island in all the thickness of the sample showing a complete interpenetration of the two polymers.

TGA analyses were performed in order to determine the influence of PPY created in the interfacial polymerization step on thermal stability of the object and characterize the amount of PPY deposited (**Figure 5**). The acidic dopants of the PPY are volatilized upon heating,[48] which explains why the PEGDA/PPY hydrogels show lower thermal stability than that of PEGDA ones below 350 °C. As expected, PEGDA/PPY hydrogel left more residue at 700 °C in comparison to the sample without PPY (Figure 5). Moreover this residue increases as the increasing of water in the initial formulation. This could be related to the fact that the more the structure is swellable, the more free space is available for PPY infiltration. This relationship between cross-linking density and the amount of water in the initial formulation could also be observed in the decrease of T_g measured by DSC. In fact, the more the hydrogel is swelled during its formation (which means the higher its water content), the lower is the cross-linking density.[49] DSC measurements were also performed on treated PEGDA/PPY samples.

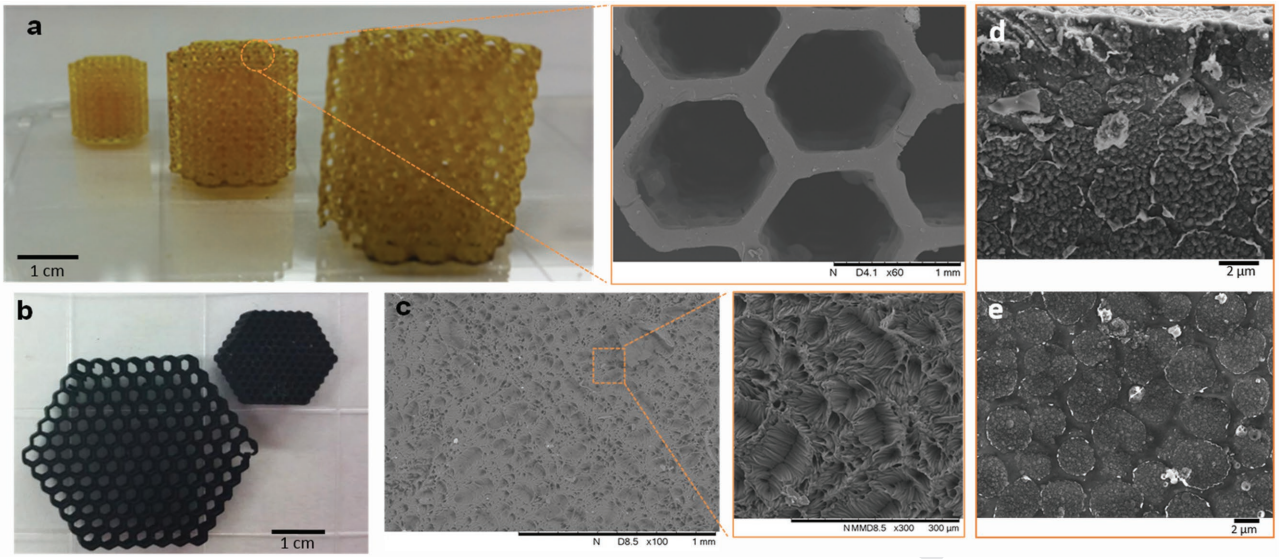

Figure 4. a) Example of a honeycomb structure printed in different dimension (PEGDA_40) and SEM detail of the features obtained. b) 3D printed PEGDA-PPY honeycomb structures. c) SEM images of the pyrrole surface. d,e) Cross section of a thick sample (4 mm).

The presence of a second polymeric phase hinders PEGDA chain mobility resulting in the increase of T_g.

XPS measurements have been performed on sample PEGDA 30_PPY surface in order to obtain information regarding the chemical composition of its first layers (≤10 nm). In **Figure 6a** we report the survey spectrum of the sample: we detected C (59.4 at%), O (26.0 at%), N (5.7 at%), and some impurities due to Cl (0.5 at%) and Si (8.5 at%). We then performed high resolution analysis on the C1s peak (as reported in Figure 6b).

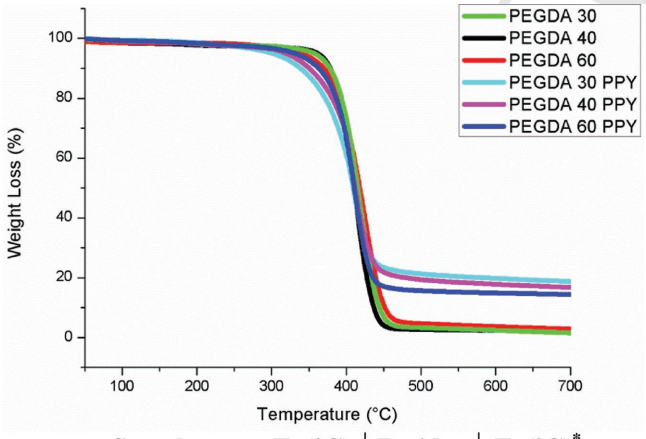

Sample	T_5 (°C)	Residue	T_g (°C)*
PEGDA_60	355	2.3	-42
PEGDA_40	360	1.5	-48
PEGDA_30	357	2.8	-50
PEGDA_60_PPY	330	14.4	-30
PEGDA_40_PPY	319	16.7	-39
PEGDA_30_PPY	301	18.7	-45

*DSC value

Figure 5. TGA plots and thermal properties of the compositions. *T_5 represents the temperature at which the 5% in weight is lost.

We attributed four components to the raw signal in order to fit properly the experimental curve. The first component at 284.5 eV has been attributed to C—C/H or α-carbons bonds,[50] the second at 286.1 eV to α-carbons, the third one at 287.4 eV to α-carbons adjacent to positively charged N atoms (Cα *), and the last one at 288.3 eV at carbon atoms bonded with oxygen species (—C=O or —COO-).[51] The same procedure has also been applied to the N1s peak (Figure 6c), obtaining four components: imine —N = (398.2 eV), amine —NH— (399.4 eV), protonated amine —NH2+- (400.1 eV), and protonated imine = NH— (401.5 eV).[52]

A further analysis has been accomplished to observe the homogeneity of PPy inclusion in the PEGDA matrix, at least in the first layers. To obtain this information we performed a depth profile measurements, using Ar+ as sputtering source. We alternated sputtering cycle (1 min) with HR measurements in the N1s region. We repeated the procedure for 60 cycles (60 min) obtaining the profile reported in Figure 6d. As can be clearly seen, the intensity of the nitrogen signal is almost constant during all the measurement. A rough estimation of the polymeric composite depth sputtered can be done according to the literature,[53] by considering a sputter rate of the order of 10 nm min^{-1} and then obtaining a 600 nm depth. Along this sputtering depth PPY distribution as expected from SEM observations.

Electrical measurements were performed on films in order to evaluate the influence of PPY on the resistivity. As reported in **Figure 7** the presence of PPY decreases the films' resistivity of one order of magnitude or more. This indicates that a continuous PPY network was successfully formed with interfacial polymerization. The resistivity values obtained are in good agreement with values reported in the literature of similar systems.[54] It is also important to underline that all the new formulations showed a resistivity considerably lower than PEGDA photocured without water.[15] Moreover, the more the water in the initial formulation, the lower the resistivity measured. In

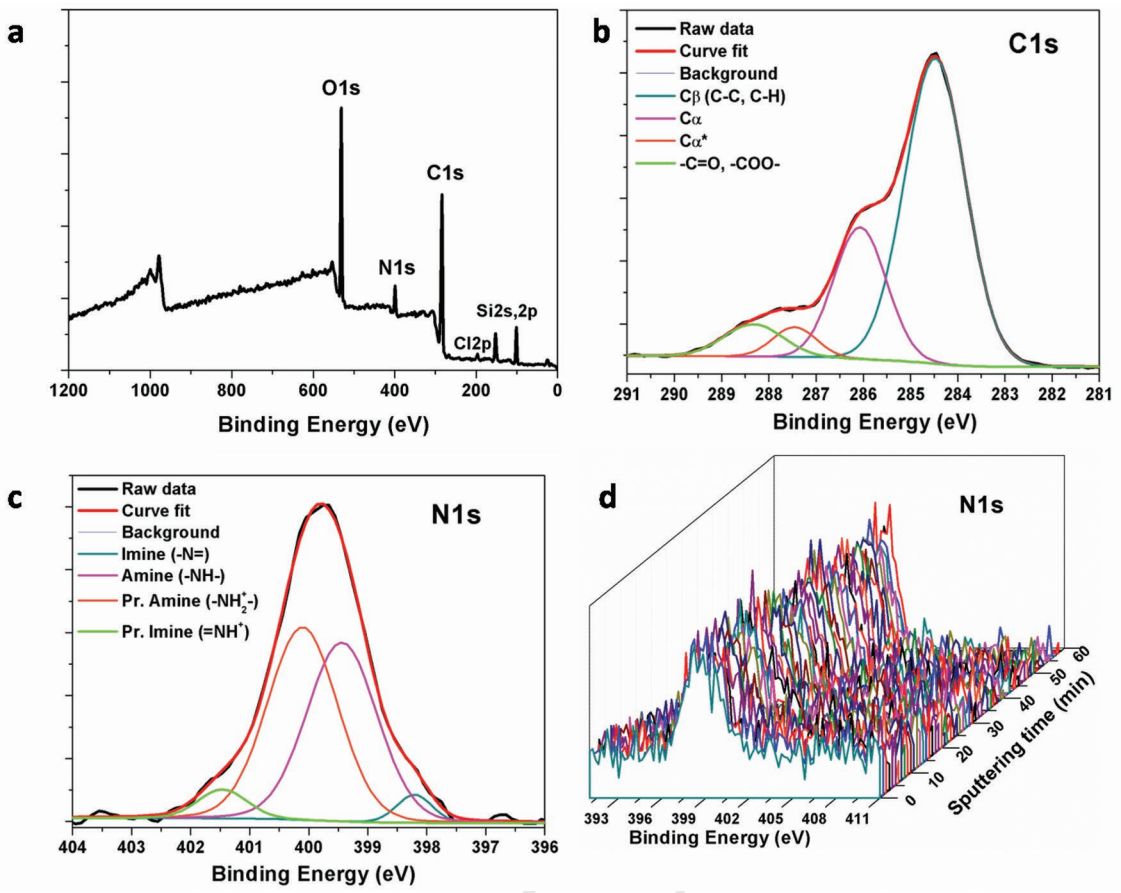

Figure 6. a) Sample PEGDA_30_PPY XPS survey spectrum; b,c) XPS high-resolution core level peaks for C1s and N1s along with their deconvolution procedure results; d) XPS depth profile curves for N1s peak (Ar+ source at 2 kV, alternate sputtering with 1 min cycle each).

order to clarify this point, electrical measurements were performed on the same neat PEGDA samples after drying in a vacuum oven overnight. All the samples showed higher resistivity (2 MΩcm), which is consistent with the literature. This let us believe that some water/humidity could remain trapped in the polymeric network during material synthesis, thus reducing resistivity. However, this assumption seems to us not sufficient to explain the low resistivity values measured for PEGDA_30 sample and more investigations are ongoing to deepen this point. The same vacuum treatment was performed on the samples with PPY, which did not show significant change in the electrical behavior.

In order to evaluate the mechanical properties of the samples, honeycomb structures were printed and tested in compression

a

Sample	ρ* (MΩ cm)	R** (kΩ)	E_c** (MPa)
PEGDA_60	140	//	1.1
PEGDA_40	19	//	0.8
PEGDA_30	0.23	//	0.5
PEGDA_60_PPY	3.5	7	1.4
PEGDA_40_PPY	0.045	3	0.9
PEGDA_30_PPY	0.013	1	0.6

* Calculated on thin film
** Calculated on 3D structure

b

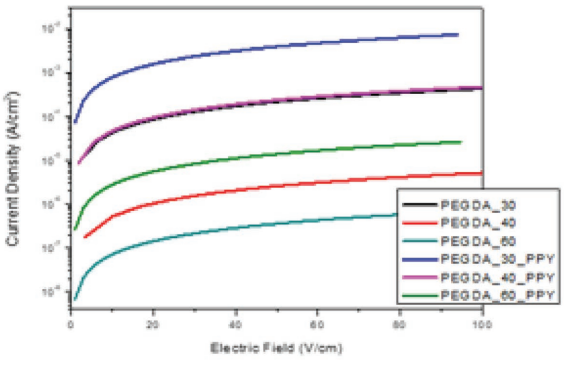

Figure 7. a) Table reporting electrical resistivity and electrical resistance and Young's modulus; b) semilogarithmic plot of *I*/*V* measurements and resistance evaluation for the different samples.

tests. The table in Figure 7a reports the Young's modulus for each formulation under compression. The measurements performed on the structures showed that the Young's modulus is higher in the presence of PPY compared to PEGDA sample without PPY, which can explain that the presence of a second phase hinders the PEGDA chain mobility as already seen in the DSC. Finally, the resistance of 3D printed conductive hydrogel structures was also measured, confirming the trend observed on films.

4. Conclusions

In this paper, we reported a novel approach for the fabrication of electrically conductive, mechanically tough 3D printed hydrogels by coupling interfacial polymerization of PPY with 3D printing technology. It was demonstrated that precise 3D structures of PEG-based hydrogels can be realized even with a considerable high amount of water in the initial formulation. The honeycomb structures were successfully infiltrated with PPY by interfacial polymerization; ATR, XPS, and SEM results indicate the existence of PPY within the matrix. Moreover the dye used for enhancing 3D printing precision was exploited for PPY doping. The developed structures were electrically conductive and mechanically tough. This strategy could be applied for developing a new bioelectronics interface for several biomedical applications.

Acknowledgements

The authors are grateful for the financial support from the Natural Science and Engineering Research Council of Canada (NSERC), the Canada Foundation for Innovation (CFI), and the University of Western Ontario.

Conflict of Interest

The authors declare no conflict of interest.

Keywords

3D printing, interfacial polymerization, PEGDA, photopolymerization

Received: July 22, 2017
Revised: November 1, 2017
Published online:

[1] G. Justin, A. Guiseppi-Elie, *Biomacromolecules* **2009**, *10*, 2539.
[2] C. J. Small, C. O. Too, G. G. Wallace, *Polym. Gels Networks* **1997**, *5*, 251.
[3] Y.-x. Zhao, K.-f. Ren, Y.-x. Sun, Z.-j. Li, J. Ji, *RSC Adv.* **2014**, *4*, 24511.
[4] A. Guiseppi-Elie, *Biomaterials* **2010**, *31*, 2701.
[5] Y. Xiao, L. He, J. Che, *J. Mater. Chem.* **2012**, *22*, 8076.
[6] J. Ji, et al., *J. Macromol. Sci., Part B: Phys.* **2015**, *54*, 1122.
[7] H. P. de Oliveira, S. A. Sydlik, T. M. Swager, *J. Phys. Chem. C* **2013**, *117*, 10270.
[8] Y. Wu, et al., *J. Mater. Chem. B* **2015**, *3*, 5352.
[9] S. Naficy, J. M. Razal, G. M. Spinks, G. G. Wallace, P. G. Whitten, *Chem. Mater.* **2012**, *24*, 3425.
[10] H. Huang, J. Wu, X. Lin, L. Li, S. Shang, M. C. Yuen, G. Yan, *Carbohydr. Polym.* **2013**, *95*, 72.
[11] C. Vallejo-Giraldo, A. Kelly, M. J. P. Biggs, *Drug Discovery Today* **2014**, *19*, 88.
[12] Y. Zhao, B. Liu, L. Pan, G. Yu, *Energy Environ. Sci.* **2013**, *6*, 2856.
[13] J. Stejskal, *Chem. Papers*, 1.
[14] Y. L. Kong, I. A. Tamargo, H. Kim, B. N. Johnson, M. K. Gupta, T.-W. Koh, H.-A. Chin, D. A. Steingart, B. P. Rand, M. C. McAlpine, *Nano Lett.* **2014**, *14*, 7017.
[15] J. N. Hanson Shepherd, S. T. Parker, R. F. Shepherd, M. U. Gillette, J. A. Lewis, R. G. Nuzzo, *Adv. Funct. Mater.* **2011**, *21*, 47.
[16] R. Suntornnond, J. An, C. K. Chua, *Macromol. Mater. Eng.* **2017**, *302*, 1600266.
[17] M. Zhou, B. H. Lee, L. P. Tan, *Int. J. Bioprint.* **2017**, *3*, 2017.
[18] J. C. McDonald, M. L. Chabinyc, S. J. Metallo, J. R. Anderson, A. D. Stroock, G. M. Whitesides, *Anal. Chem.* **2002**, *74*, 1537.
[19] B. C. Gross, J. L. Erkal, S. Y. Lockwood, C. Chen, D. M. Spence, *Anal. Chem.* **2014**, *86*, 3240.
[20] J. Z. Manapat, Q. Chen, P. Ye, R. C. Advincula, *Macromol. Mater. Eng.* **2017**, *302*, 1600553.
[21] X. Wang, Q. Guo, X. Cai, S. Zhou, B. Kobe, J. Yang, *ACS Appl. Mater. Interfaces* **2014**, *6*, 2583.
[22] E. Fantino, A. Chiappone, F. Calignano, M. Fontana, F. Pirri, I. Roppolo, *Materials* **2016**, *9*, 589.
[23] A. Chiappone, E. Fantino, I. Roppolo, M. Lorusso, D. Manfredi, P. Fino, C. F. Pirri, F. Calignano, *ACS Appl. Mater. Interfaces* **2016**, *8*, 5627.
[24] E. Fantino, A. Chiappone, I. Roppolo, D. Manfredi, R. Bongiovanni, C. F. Pirri, F. Calignano, *Adv. Mater.* **2016**, *28*, 3712.
[25] S. Stassi, E. Fantino, R. Calmo, A. Chiappone, M. Gillono, D. Scaiola, C. F. Pirri, C. Ricciardi, A. Chiadò, I. Roppolo, *ACS Appl. Mater. Interfaces* **2017**, *9*, 19193.
[26] J. Malda, J. Visser, F. P. Melchels, T. Jüngst, W. E. Hennink, W. J. Dhert, J. Groll, D. W. Hutmacher, *Adv. Mater.* **2013**, *25*, 5011.
[27] J.-Y. Sun, X. Zhao, W. R. Illeperuma, O. Chaudhuri, K. H. Oh, D. J. Mooney, J. J. Vlassak, Z. Suo, *Nature* **2012**, *489*, 133.
[28] N. B. Graham, in *Poly(Ethylene Glycol) Chemistry: Biotechnical and Biomedical Applications* (Ed: J. M. Harris), Springer, Boston, MA **1992**, pp. 263–281.
[29] J. M. Harris, *Poly (Ethylene Glycol) Chemistry: Biotechnical and Biomedical Applications*, Springer Science & Business Media, Berlin, Germany **2013**.
[30] K. Arcaute, L. Ochoa, F. Medina, C. Elkins, B. Mann, R. Wicker, *MRS Online Proceedings Library* **2005**, *874*.
[31] V. Chan, J. H. Jeong, P. Bajaj, M. Collens, T. Saif, H. Kong, R. Bashir, *Lab Chip* **2012**, *12*, 88.
[32] V. Chan, P. Zorlutuna, J. H. Jeong, H. Kong, R. Bashir, *Lab Chip* **2010**, *10*, 2062.
[33] A. Chiappone, I. Roppolo, E. Naretto, E. Fantino, F. Calignano, M. Sangermano, F. Pirri, *Composites, Part B: Eng.* **2017**, *124*, 9.
[34] X. Wang, M. Jiang, Z. Zhou, J. Gou, D. Hui, *Composites, Part B: Eng.* **2017**, *110*, 442.
[35] N. Nuraje, K. Su, *ACS Nano* **2008**, *2*, 502.
[36] G. Qi, Z. Wu, H. Wang, *J. Mater. Chem. C* **2013**, *1*, 7102.
[37] J. Bhadra, D. Sarkar, *Indian J. Phys.* **2010**, *84*, 1321.
[38] D. Zhang, F. Di, Y. Zhu, Y. Xiao, J. Che, *J. Bioact. Compat. Polym.: Biomed. Appl.* **2015**, *30*, 600.
[39] N. V. Blinova, M. Trchová, J. Stejskal, *Eur. Polym. J.* **2009**, *45*, 668.
[40] M. Karbarz, M. Gniadek, M. Donten, Z. Stojek, *Electrochem. Commun.* **2011**, *13*, 714.

[41] X. Tuo, B. R. Li, C. L. Chen, Z. L. Huang, H. B. Huang, L. Li, *Synth. Met.* **2016**, *213*, 73.
[42] S. Ying, W. Zheng, B. Li, X. She, H. Huang, L. Li, Z. Huang, Y. Huang, Z. Liu, X. Yu, *Synth. Met.* **2016**, *218*, 50.
[43] N. Saengchairat, T. Tran, C.-K. Chua, *Virtual Phys. Prototyping* **2017**, *12*, 31.
[44] J. Feng, W. Yan, L. Zhang, *Microchim. Acta* **2009**, *166*, 261.
[45] X. Yang, Z. Zhu, T. Dai, Y. Lu, *Macromol. Rapid Commun.* **2005**, *26*, 1736.
[46] H. Tai, W. Wang, T. Vermonden, F. Heath, W. E. Hennink, C. Alexander, K. M. Shakesheff, S. M. Howdle, *Biomacromolecules* **2009**, *10*, 822.
[47] A. A. Jatratkar, J. B. Yadav, R. Deshmukh, H. C. Barshilia, V. Puri, *J. Phys. Chem. Solids* **2015**, *80*, 78.
[48] Y. Liao, T. P. Farrell, G. R. Guillen, M. Li, J. A. T. Temple, X.-G. Li, E. M. V. Hoek, R. B. Kaner, *Mater. Horiz.* **2014**, *1*, 58.
[49] L. M. Weber, C. G. Lopez, K. S. Anseth, *J. Biomed. Mater. Res., Part A* **2009**, *90*, 720.
[50] P. M. Carrasco, M. Cortazar, E. Ochoteco, E. Calahorra, J. A. Pomposo, *Surf. Interface Anal.* **2007**, *39*, 26.
[51] N. Garino, A. Sacco, M. Castellino, J. A. Muñoz-Tabares, A. Chiodoni, V. Agostino, V. Margaria, M. Gerosa, G. Massaglia, M. Quaglio, *ACS Appl. Mater. Interfaces* **2016**, *8*, 4633.
[52] S. Golczak, A. Kanciurzewska, M. Fahlman, K. Langer, J. J. Langer, *Solid State Ionics* **2008**, *179*, 2234.
[53] T. Nobuta, T. Ogawa, *J. Mater. Sci.* **2009**, *44*, 1800.
[54] G. Kaur, R. Adhikari, P. Cass, M. Bown, P. Gunatillake, *RSC Adv.* **2015**, *5*, 37553.

Query

Q1: Please provide TOC keyword.

Q2: Please provide the highest academic title (either Dr. or Prof.) for all authors, where applicable.

Q3: Please define 'ATR and FTIR' at the first occurrence in the text.

Q4: Please define 'HR' at the first occurrence in the text.

Q5: Please confirm if the deletion of panel (a) from the caption of Figure 3 is correct.

Q6: Please check that the edits to the sentence 'The same procedure has also been applied ...' are OK and that the meaning has not been changed.

Q7: Please complete the sentence 'Along this sputtering depth PPY distribution as expected from SEM observations'.

Q8: Please check that the edits to the sentence 'However, this assumption seems to us not sufficient ...' are OK and that the meaning has not been changed.

Q9: Please check that the edits to the sentence 'The measurements performed on the structures ...' are OK and that the meaning has not been changed.

Q10: Please check that the edits to the sentence 'The honeycomb structures were successfully ...' are OK and that the meaning has not been changed.

Q11: The term 'et al.' is not permitted in the reference list. Please provide all author names in references (6).

Q12: Please confirm if the authors in refs. (10, 14, 15, 18, 21–27, 31, 33, 41, 42, 46–48, and 51) are correct as included.

Q13: Please provide year of publishing and volume number in ref. (13).

Q14: Please confirm if the year and volume number in ref. (20) are correct as included.

Q15: Please confirm if the publisher name is correct as edited in ref. (28).

Q16: Please confirm if the publisher location in ref. (29) is correct as included.

Q17: Please provide page number in ref. (30), if available.

Macromolecular Materials and Engineering

Editorial office:
Wiley-VCH Verlag
Boschstraße 12, 69469 Weinheim
Germany

Tel.: +49 (0) 6201 – 606 – 581
Fax: +49 (0) 6201 – 606 – 510
Email: macromol@wiley-vch.de

Reprint Order Form 2018

Short DOI: mame._____

Please send me and bill me for

☐ **Reprints** via ☐ airmail (+ 25 Euro)
☐ surface mail

Please send me and bill me for a:

☐ **high-resolution PDF file** (330 Euro).

My Email address:

_____

Please note: It is not permitted to present the PDF file on the internet or on company homepages.

Information regarding VAT

Please note that from German sales tax point of view, the charge for **Reprints, Issues or Posters** is considered as **"supply of goods"** and therefore, in general, such delivery is a subject to German sales tax. However, this regulation has no impact on customers located outside of the European Union. Deliveries to customers outside the Community are automatically tax-exempt. Deliveries within the Community to institutional customers outside of Germany are exempted from the German tax (VAT) only if the customer provides the supplier with his/her VAT number. The VAT number (value added tax identification number) is a tax registration number used in the countries of the European Union to identify corporate entities doing business there. It starts with a country code (e.g. FR for France, GB for Great Britain) and follows by numbers.

VAT no.: _____

(Institutes / companies in EU countries only)

Purchase Order No.: _____

Delivery address / Invoice address:
Name of recipient, University, Institute, Street name and Street number, Postal Code, Country

_____

_____

_____

_____

_____

_____

_____

Date and Signature: _____

Credit Card Payment (optional) - You will receive an invoice.

VISA, MasterCard, AMERICAN EXPRESS

Please use the Credit Card Token Generator located at the website below to create a token for secure payment. The token will be used instead of your credit card number.

Credit Card Token Generator:
https://www.wiley-vch.de/editorial_production/index.php

Please transfer your token number to the space below.

Credit Card Token Number

Price list for reprints (The prices include mailing and handling charges. All Wiley-VCH prices are exclusive of VAT)

No. of pages	Price (in Euro) for orders of					
	50 copies	100 copies	150 copies	200 copies	300 copies	500 copies
1-4	345	395	425	445	548	752
5-8	490	573	608	636	784	1077
9-12	640	739	786	824	1016	1396
13-16	780	900	958	1004	1237	1701
17-20	930	1070	1138	1196	1489	2022
for every additional 4 pages	147	169	175	188	231	315

Wiley-VCH Verlag GmbH & Co. KGaA; Location of the Company: Weinheim, Germany;
Trade Register: Mannheim, HRB 432833, Chairman of the Board: Mark Allin
General Partner: John Wiley & Sons GmbH, Location: Weinheim, Germany
Trade Register Mannheim, HRB 432296,
Managing Directors: Sabine Steinbach, Dr. Guido F. Herrmann

WILEY-VCH